BULLETIN OF THE POLISH ACADEMY OF SCIENCES
TECHNICAL SCIENCES, Vol. 69(5), 2021, Article number: e138814
DOI: 10.24425/bpasts.2021.138814

Specific emitter identification based on one-dimensional complex-valued residual networks with an attention mechanism

Lingzhi QU, Junan YANG*, Keju HUANG, and Hui LIU

College of Electronic Engineering, National University of Defense Technology, Hefei, Anhui 230037, People's Republic of China

Abstract. Specific emitter identification (SEI) can distinguish single-radio transmitters using the subtle features of the received waveform. Therefore, it is used extensively in both military and civilian fields. However, the traditional identification method requires extensive prior knowledge and is time-consuming. Furthermore, it imposes various effects associated with identifying the communication radiation source signal in complex environments. To solve the problem of the weak robustness of the hand-crafted feature method, many scholars at home and abroad have used deep learning for image identification in the field of radiation source identification. However, the classification method based on a real-numbered neural network cannot extract In-phase/Quadrature (I/Q)-related information from electromagnetic signals. To address these shortcomings, this paper proposes a new SEI framework for deep learning structures. In the proposed framework, a complex-valued residual network structure is first used to mine the relevant information between the in-phase and orthogonal components of the radio frequency baseband signal. Then, a one-dimensional convolution layer is used to a) directly extract the features of a specific one-dimensional time-domain signal sequence, b) use the attention mechanism unit to identify the extracted features, and c) weight them according to their importance. Experiments show that the proposed framework having complex-valued residual networks with attention mechanism has the advantages of high accuracy and superior performance in identifying communication radiation source signals.

Key words: complex-valued residual network; specific emitter identification; fingerprint characteristic; attention mechanism; one-dimensional convolution.

1. INTRODUCTION

Specific emitter identification (SEI) is the process of uniquely identifying an individual emitter from the same class of communication radiation sources by its individual properties that arise from hardware imperfections [1]. The characteristics of electronic circuits and radio frequency (RF) components determined by the production and manufacturing processes make the SEI of communication equipment achievable [2]. Its unique characteristics and resistance to fraud also play an important role in situational awareness in military communications, electronic reconnaissance, and battlefield networks [3–5].

The key to SEI is to extract features that represent hardware variability, also known as RF fingerprints. Numerous methods have been suggested for RF fingerprints. The transient-based method extracts features from the on/off transient of the signal [6–9], but the signal has a short duration and is challenging to extract. The feature-extraction method is based on time-frequency analysis and on the time-frequency energy distribution characteristics of individual signals of different radiation sources; it compares the observed with the ideal signals [10–13]. The method based on modulation analysis compares the constellation diagram of the received signal with the ideal constellation diagram and uses the constellation diagram deviation generated in the modulation process as the fingerprint feature of the radiator [14–15]. The method based on nonlinear dynamics takes the emitter as a nonlinear dynamic system and extracts the RF characteristics [16–18]. In addition, other research studies have extracted RF fingerprints from Symbol Synchronization [4], graphical representations [19], or geometrical features [20,21]. Some methods extract features from fingerprint mechanisms [22] or time-varying channel conditions [23]. The applications of SEI technology in modern identification models continue to evolve, such as radar emitter recognition systems for electronic intelligence systems [24] and device identification methods to increase the security of the Internet of Things [25]. Most previous research studies on SEI were based on artificial characteristics and depended on prior knowledge of signal characteristics and existing signal processing tools [26]. In turn, prior knowledge was related to the specific attributes of the received signal [27], in which the extracted features were relatively single and required high feature effectiveness. With the increasing complexity of the actual electromagnetic (EM) environment and the tremendous increase in communication signals, it is difficult to obtain effective prior information. Correspondingly, this has led to the increase of classification error.

In recent years, deep learning has made significant breakthroughs in computer vision, speech recognition, and face recognition and has been compared with traditional methods based on the manual extraction of features, whereby deep learning algorithms learn features from data. Deep learning has demonstrated superior performance in many fields. Therefore, some

*e-mail: yangjunan@ustc.edu

Manuscript submitted 2021-03-23, revised 2021-05-31, initially accepted for publication 2021-07-16, published in October 2021

researchers have recently begun to explore the application of deep learning in SEI. Shieh proposed a three-layer vector neural network for emitter identification [5]. Zhang applied convolutional neural networks (CNNs) to radio cognition [28]. West input two-way I/Q signals directly to a deep CNN to classify radio signals of different modulation classes [29]. Wu used a recurrent neural network (RNN) based on long-and short-term memory for RF fingerprint identification and achieved high-detection accuracy even in the presence of high-noise-power levels [30]. Ding used a CNN in a bispectrum with higher accuracy than those associated with conventional methods [31]. Pan constructed a deep residual network based on a Hilbert spectrum image, and the simulation results showed that the method performed well under various channel conditions [26]. Baldini compared various methods for converting signals into images as CNN inputs, including recurrence plots, continuous wavelet transform (CWT), and short-time Fourier transform (STFT). Experiments showed that the wavelet-based method outperformed the other methods [32]. Huang proposed a CWT-based approach and domain adversarial neural networks (DANN) to improve the performance of SEIs at various frequencies [33]. Bin combined attention mechanisms and CNNs to improve the identification of individuals from radiation sources [34].

O'Shea *et al*. were the first to propose a two-channel real-numbered network for EM signal waveform identification in a complex domain [35]. This approach solved the input problem of complex waveform signals but could not extract the I/Q-related information from EM signals [36]. Hirosc *et al*. demonstrated that complex networks could effectively extract I/Q-related information in EM signal waveforms through I/Q fusion channels, thus effectively improving the identification accuracy of EM signals [37]. Trabelsi *et al*. proposed the derivation of a systematic formulation of a complex-valued neural network composed of basic components and constructed complex residual networks based on the Keras framework [38]. Wang applied deep residual networks to RF fingerprint identification and achieved better identification results [39].

However, in the field of signal identification of communication radiation sources, most of the sampled communication signals are one-dimensional (1D), time-domain sequences. If the original, two-dimensional network model is used directly, additional computation time and storage space will be required to convert the 1D to a two-dimensional (2D) sequence. In addition, the dimensional transformation of a 1D time-domain sequence to a 2D sequence in practical applications leads to poor real-time performance. Although the complex-valued residual network model can extract fingerprint features of radiation sources using the in-phase and orthogonal components of the signal, the weights of the features are not the same. This means that redundant and useless features will suppress the identification accuracy. This paper proposes novel, 1D, complex-valued residual networks with attention mechanism (CVResNet-1D-AM), which input the collected time-domain data of the I and Q channels into the network, extracts features from the original communication signal sequence directly, and uses the attention mechanism to identify the key information of the extracted features for communication radiation source signal identification.

In summary, our contributions are the following:

- Based on the PyTorch framework, we constructed a complex-valued residual network to improve the generalization of the network model. Compared with the real-numbered residual neural network, the number of model parameters of the complex-valued residual network is smaller, and the operation time is shorter.
- The 1D convolutional layer can extract features directly from the time-domain sequence of communication signals and save dimensional change time, which leads to better real-time performance.
- We have added a unit that uses the attention mechanism that can automatically weigh the feature maps generated by the 1D convolutional layers such that important features gain more weight while suppressing features that negatively impact identification. The experimental results show that the CVResNet-1D-AM proposed in this study has higher accuracy and better identification performance in the identification of communication radiation source signals.

The remainder of this paper is structured as follows: in Section 2, the complex-valued residual network model under the PyTorch framework is introduced, and Section 3 details the proposed CVResNet-1D-AM using 1D convolution and attention mechanism. Section 4 presents the identification results and discusses them using two real sample sets. The conclusions are presented in Section 5.

2. COMPLEX-VALUED RESIDUAL NETWORK

To implement the traditional two-dimensional real-valued convolution on the complex domain, we used the complex vector $z = x + iy$ to convolve the complex filter matrix $W = a + iB$, where a and B are real-numbered matrices, and x and y are real-numbered vectors.

$$W * z = (\boldsymbol{A} * \boldsymbol{x} - \boldsymbol{B} * \boldsymbol{y}) + i(\boldsymbol{B} * \boldsymbol{x} - \boldsymbol{A} * \boldsymbol{y}). \tag{1}$$

Using the matrix form for the expression, the real and imaginary parts of the operation can be expressed as

$$\begin{bmatrix} R(W * z) \\ V(W * z) \end{bmatrix} = \begin{bmatrix} \boldsymbol{A} & -\boldsymbol{B} \\ \boldsymbol{B} & \boldsymbol{A} \end{bmatrix} * \begin{bmatrix} \boldsymbol{x} \\ \boldsymbol{y} \end{bmatrix}. \tag{2}$$

The major advantage of the complex-valued network compared with the real number network is that the correlation information between the in-phase and orthogonal components of the RF baseband signal can be fully extracted; in other words, the nonlinear characteristics of the transmitter RF fingerprint can be fully extracted. However, it was found that the gradual increase in the number of network layers in the complex-valued network also caused additional error increases and led to the gradient dispersion problem that yielded poor identification and classification results. To solve this problem, we replaced the real-numbered network structures, such as the real-numbered convolutional layer, real-numbered batch normalization and pooling layer with the complex-valued network structures, such as the

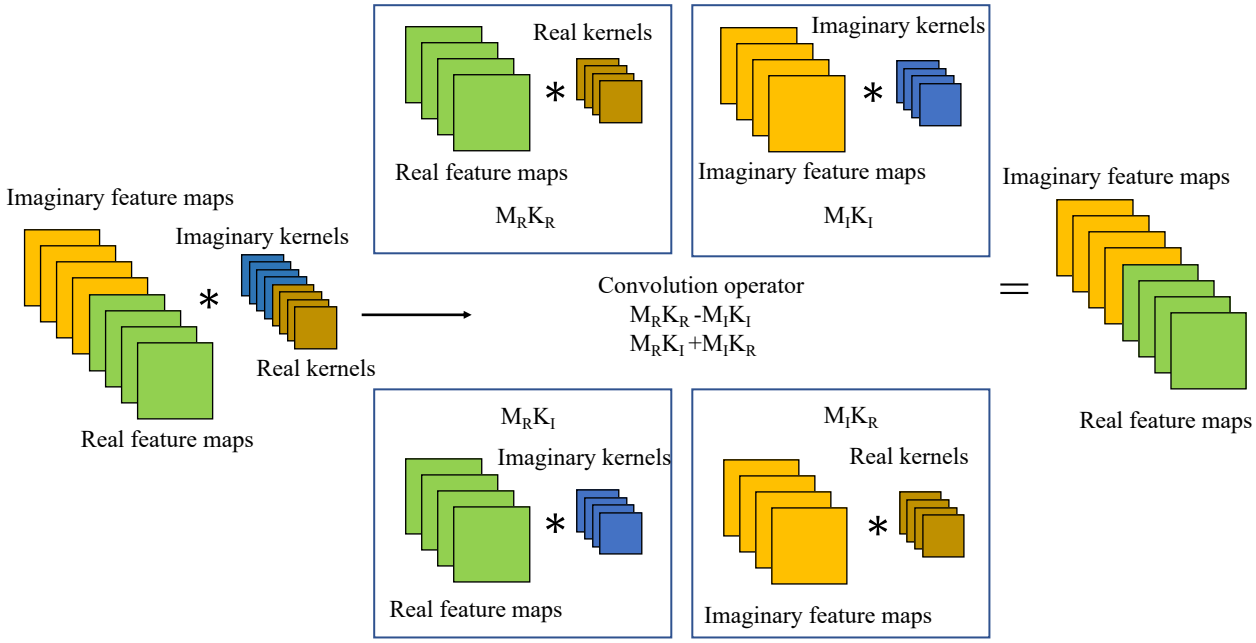

Fig. 1. Complex-valued convolution process

complex-valued convolutional layer, batch normalization, and pooling layer, and we constructed the complex-valued residual stack based on the PyTorch framework.

$$H(x_r, x_i) = x_r, x_r + F(x_r, x_i), \tag{3}$$

where x_r, x_i are the inputs of the residual unit, $F(x_r, x_i)$ is the output of the data after the convolution layer, and $H(x_r, x_i)$ is the output of the residual unit.

For complex-valued convolution, we considered a typical real-valued 2D convolution layer with N feature mappings, where N is divisible by the number two. We assigned the first N/2 feature mappings to represent the real components to express these feature mappings as complex numbers. The remaining N/2 feature mappings were used to represent the imaginary components. Therefore, for a four-dimensional weight tensor W that connects Nin input feature mappings to Nout output feature mappings with a convolution kernel with a size of m×m, we obtained a weight tensor with a complex weight with a size of (Nout×Nin×m×m)/2. In contrast to the common 2D residual networks, and because the communication radiation source signal is a 1D time series similar to a residual neural network, the framework of the 1D complex-valued residual network we constructed is as follows.

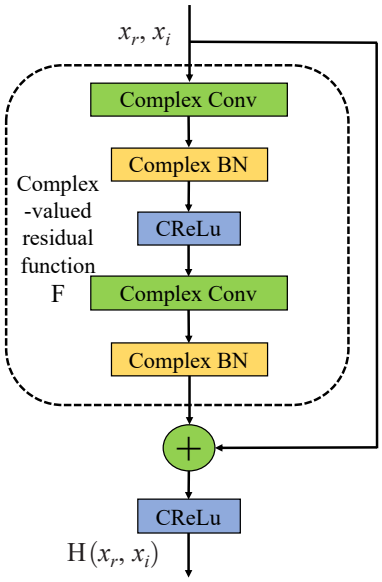

Fig. 2. Complex-valued residual structure

Table 1
Network framework

Layer name	ResNet-1D 18-layer	ResNet-1D 34-layer	CVResNet-1D
Conv1	7×7, 64, stride2	7×7, 64, stride2	7×7, 32, stride2
	3×3 max pool, stride2		
conv2_x	$\begin{bmatrix}3\times3 & 64\\ 3\times3 & 64\end{bmatrix}\times2$	$\begin{bmatrix}3\times3 & 64\\ 3\times3 & 64\end{bmatrix}\times3$	$\begin{bmatrix}3\times3 & 32\\ 3\times3 & 32\end{bmatrix}\times3$
conv3_x	$\begin{bmatrix}3\times3 & 128\\ 3\times3 & 128\end{bmatrix}\times2$	$\begin{bmatrix}3\times3 & 128\\ 3\times3 & 128\end{bmatrix}\times4$	$\begin{bmatrix}3\times3 & 64\\ 3\times3 & 64\end{bmatrix}\times4$
conv4_x	$\begin{bmatrix}3\times3 & 256\\ 3\times3 & 256\end{bmatrix}\times2$	$\begin{bmatrix}3\times3 & 256\\ 3\times3 & 256\end{bmatrix}\times6$	$\begin{bmatrix}3\times3 & 128\\ 3\times3 & 128\end{bmatrix}\times6$
conv5_x	$\begin{bmatrix}3\times3 & 512\\ 3\times3 & 512\end{bmatrix}\times2$	$\begin{bmatrix}3\times3 & 512\\ 3\times3 & 512\end{bmatrix}\times3$	$\begin{bmatrix}3\times3 & 256\\ 3\times3 & 256\end{bmatrix}\times3$
	Average pool, fully connected layer, SoftMax		

3. ONE-DIMENSIONAL CONVOLUTIONAL NEURAL NETWORK WITH AM

3.1. One-dimensional convolution

Convolutional layers are typically used to process 2D data. Because the communication radiation source signal is mainly stored in 1D, and the dimensional transformation is time-consuming, this paper proposes using a 1D convolutional layer for feature extraction. Compared with the traditional 2D convolutional layer, the 1D convolutional layers reduces the number of parameters. Moreover, the 1D signal in the time domain is no longer converted into a 2D feature map, which saves computation time and storage space. The details of the process for the 1D convolution are shown in Fig. 3.

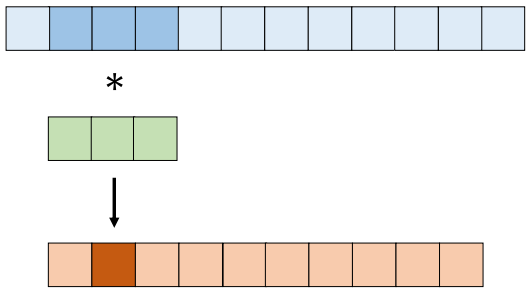

Fig. 3. One-dimensional convolution operation

The mathematical expression of 1D convolution operation is as follows:

$$x_q^l = f\left(u_q^l\right), \tag{4}$$

$$u_q^l = \sum_{p \in \mathrm{M}_q} x_p^{l-1} * k_{pq}^l + b_q^l. \tag{5}$$

In equations (4) and (5), the superscript $l = 1, 2, \ldots, N$ represents the lth layer of convolution, x_q^l is the activation value output by the q channel of the convolutional layer l, $f(\cdot)$ is the activation function of the network, u_q^l is the net activation of the q channel output of the convolutional layer l, x_p^{l-1} is the output of the convolutional layer $l-1$, k_{pq}^l is the convolutional kernel function of the pth input feature vector corresponding to the qth channel of the convolutional layer l, and b_q^l is the offset of the q channel of the convolutional layer l.

3.2. Convolutional block attention module

The convolutional block attention module (CBAM) [40] focuses on capturing key information from the data by simulating the visual perception of the human eye and by selectively focusing on salient features. CBAM studies have demonstrated that the sequence of the channel attention module followed by the spatial attention module performs better. In this study, we propose a 1D attention mechanism (AM) similar to the original CBAM. AM is added between the last pooling layer and the first fully connected layer; it helps capture features and suppresses less important information. The proposed AM structure is shown in Fig. 4.

From one viewpoint, Fig. 5 shows that the channel attention module can focus on features' key channel location information and achieve optimized feature classification by extracting the importance of different channel features. Channel attention can tap the dependency relationship between channel maps to determine the importance of each feature channel and assign different weights. There is an intrinsic connection between two-way IQ signals for radio signals, and the feature maps of different channels can reflect parts of the subtle features of radio data. Correspondingly, channel attention can be used to suppress useless features and improve the classification and identification effect.

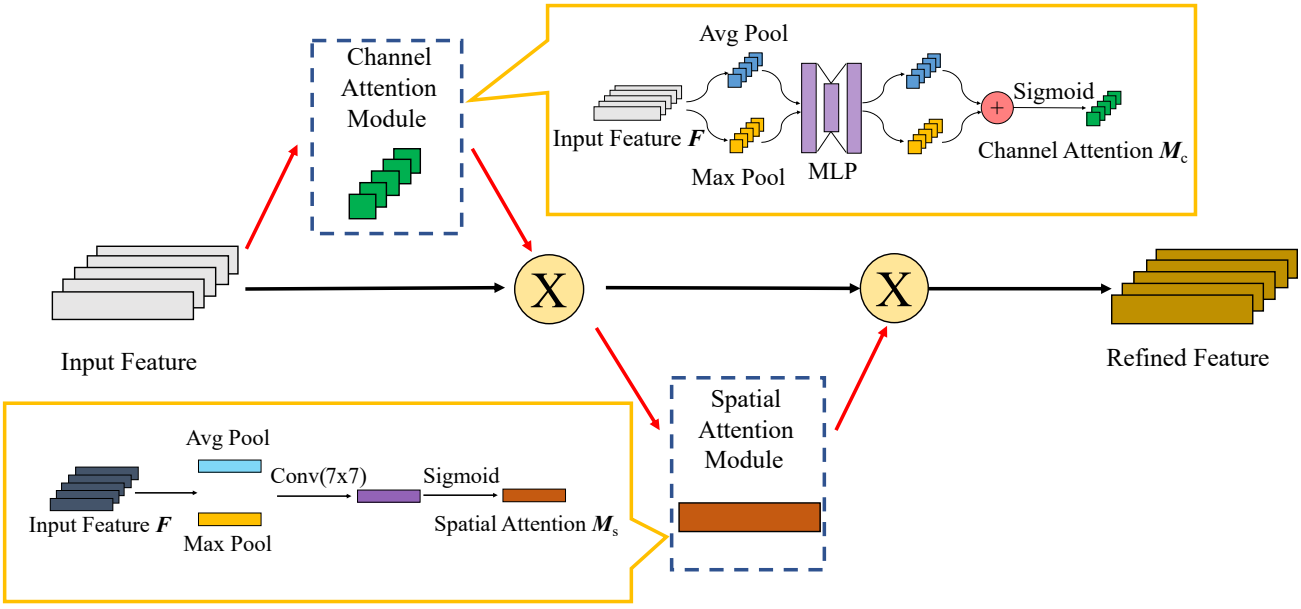

Fig. 4. Attention mechanism

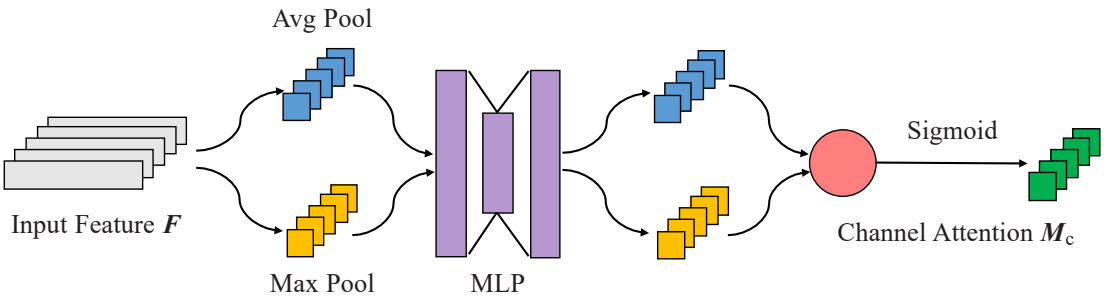

Fig. 5. Channel attention module

For 1D radio data in the channel attention module, let the input feature set $F \in \mathbf{R}^{H\times C}$; after the average pooling layer and the maximum pooling layer, we can obtain $F_{\text{avg}} \in \mathbf{R}^{1\times C}$ and $F_{\max} \in \mathbf{R}^{1\times C}$.

$$F_{\text{avg}} = \text{Averagepool}(F) = \frac{1}{W}\sum_{i}^{W} F(i, C), \tag{6}$$

$$F_{\max} = \text{Maxpool}(F) = \max\left(F(1 \le i \le W)C\right). \tag{7}$$

With the use of a multilayer perceptron (MLP), the parameters in the MLP are shared, the number of neurons in the hidden layer is C/r, and the number of neurons in the output layer is C. We sum up the two feature maps corresponding to the output, then use the sigmoid function to activate the feature maps obtained by the summation to obtain the channel attention weight coefficient $M_c(F) \in \mathbf{R}^{1\times C}$, and finally multiply the weight coefficient M_c and F to obtain the channel attention refinement output feature F'.

$$\begin{aligned} M_c(F) &= \sigma\left(\text{MLP}(\text{Avgpool}(F)) + \text{MLP}(\text{Maxpool}(F))\right) \\ &= \sigma\left(W_1\left(W_0(F_{\text{avg}})\right) + W_1\left(W_0\left(F_{\max}\right)\right)\right), \end{aligned} \tag{8}$$

$$\begin{aligned} F' &= M_c(F) \otimes F \\ &= \sigma\left(W_1\left(W_0\left(F_{\text{avg}}\right)\right) + W_1\left(W_0\left(F_{\max}\right)\right)\right) \otimes F, \end{aligned} \tag{9}$$

where σ represents the sigmoidal function, and $W_0 \in \mathbf{R}^{C/r\times C}$ and $W_1 \in \mathbf{R}^{C/r\times C}$ represent the multilayer perceptron hidden layer and output layer weights, respectively.

The channel attention weight coefficients can be regarded as feature detectors for the feature vectors of different channels. Each channel in the feature map is assigned a weight value using the channel attention weight coefficients. As the information introduced by the channel becomes more useful, the corresponding weight is obtained.

Figure 6 shows the spatial attention module. This module focuses attention on the key spatial location information of the features. It enables the network to learn the feature location information that is useful for the classification task by assigning different weights to the location information of the features. In radio signals, contextual information plays an important role in feature classification because it contains associative information. The spatial attention module enriches the contextual relationships by modeling local features and enhances the representation of radio fingerprint features.

In the spatial attention module, suppose that the input feature $F' \in \mathbf{R}^{W\times C}$ is compressed by the average pooling layer and the maximum pooling layer to obtain $F'_{\text{avg}} \in \mathbf{R}^{W\times 1}$ and $F'_{\max} \in \mathbf{R}^{W\times 1}$

$$F'_{\text{avg}} = \text{Averagepool}\left(F'\right) = \frac{1}{C}\sum_{j}^{C} F'(W, j), \tag{10}$$

$$F'_{\max} = \text{Maxpool}\left(F'\right) = \max\left(F'(W, 1 \le j \le C)\right), \tag{11}$$

The two 1D channel feature maps are then spliced together, and the spliced feature maps are compressed with the use of a 7×7 size convolutional kernel to obtain a feature map with the size of $W\times 1$. Subsequently, the sigmoidal function activates the feature map to obtain the channel attention weight coefficient $M_s(F') \in \mathbf{R}^{W\times 1}$. Correspondingly, we multiply the weight coefficient, M_s and F' to obtain the output feature F''

$$\begin{aligned} M_s(F') &= \sigma\left(f^{7\times 7}\left(\left[\text{Avgpool}(F');\ \text{Maxpool}(F')\right]\right)\right) \\ &= \sigma\left(f^{7\times 7}\left(\left[F'_{\text{avg}}; F'_{\max}\right]\right)\right), \end{aligned} \tag{12}$$

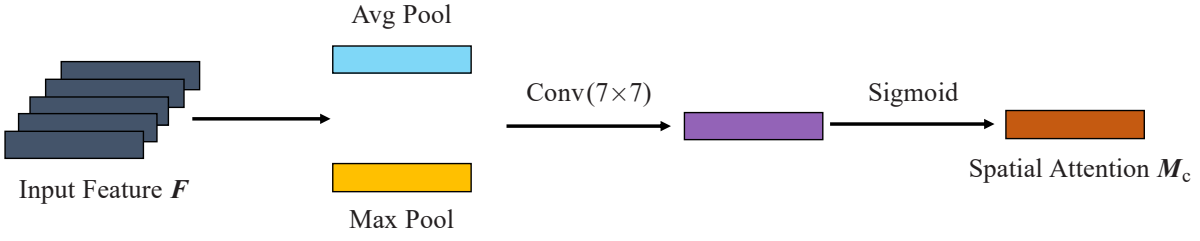

Fig. 6. Spatial attention module

where σ represents the sigmoidal function, and $f^{7\times7}$ represents a convolutional kernel with a size of 7.

The spatial attention weight coefficient reflects the importance of the different regional features. Not all areas are equally important for the identification task in the feature map. The areas related to the identification task are more worthy of attention, and this part of the area should have a greater weight.

The overall attention unit used in this study can be summarized as an input feature $F \in \mathbf{R}^{H\times C}$. First, we obtain the channel weight coefficient M_c through the channel AM, and then multiply it by the input feature to obtain a feature map F' that accurately reflects the crucial channel information of the features. Second, we use the input F' as the spatial attention module to obtain the spatial weight coefficient M_s. Finally, we multiply it by F' to obtain a feature map F'' containing channel and spatial position information.

We use the following formula to express the overall flow of the AM module:

$$\begin{aligned} F'' &= M_s(F') \otimes F' \\ &= M_s(M_c(F) \otimes F) \otimes (M_c(F) \otimes F). \end{aligned} \tag{13}$$

3.3. CVResNet-1D-AM

Based on the 1D convolution and attention unit analysis, we propose a 1D CVResNet-1D-AM with an AM, as shown in Fig. 7.

As shown in Fig. 7, the input layer is a one-dimensional time-domain sequence that uses communication signals, and the output layer refers to a layer with a certain number of neurons, that is, the number of signal types. The layout of the CVResNet-1D-AM network is such that each of the four 1D residual stacks contain three, four, six, and three identical residual units, respectively (Table 2).

Table 2
CVResNet-1D-AM Network Layout

Network structure	Output dimension	
	X_r	X_i
Input layer	1×8192	1×8192
Complex convolutional layer	32×4096	32×4096
Plural maximum pooling layer	32×2048	32×2048
One-dimensional residual stack 1	32×2048	32×2048
One-dimensional residual stack 2	64×1024	64×1024
One-dimensional residual stack 3	128×512	128×512
One-dimensional residual stack 4	256×256	256×256
Attention unit	256×256	
Complex average pooling layer	256×1	
Flat layer	256	
Fully connected layer	8	
Normalized layer	8	

We extract the envelope x of the two signal components after complex residual stack processing. The signal envelope contains important information that reflects the characteristics of the radiation source, and we then input x in the attention mechanism to obtain important features while suppressing a fewer number of important information to improve the identification effect.

$$x = \sqrt{(x_r)^2 + (x_i)^2}. \tag{14}$$

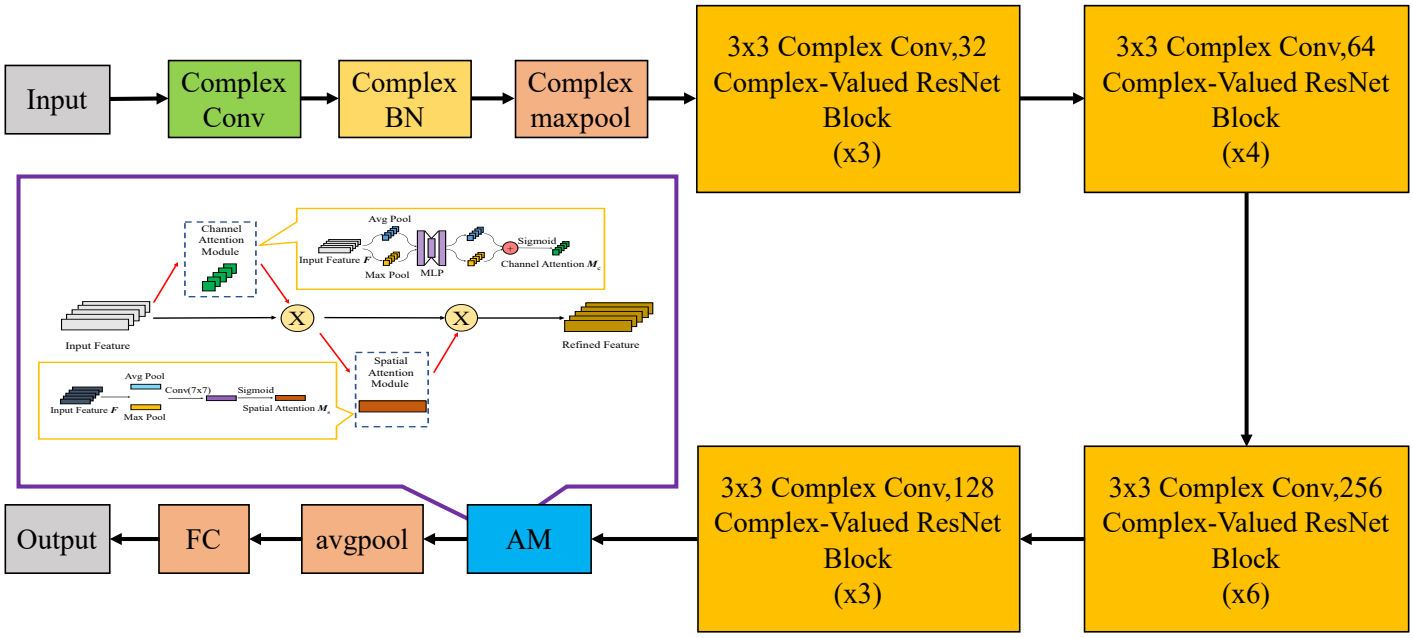

Fig. 7. CVResNet-1D-AM

4. PERSONAL IDENTIFICATION OF COMMUNICATION RADIATOR SOURCE BASED ON COMPLEX-VALUED RESIDUAL NETWORK

4.1. Experimental data

The experimental data were generated by the same type of radio communication, passed through the channel simulator, and finally collected by the same receiving device. The signal was divided in the I and Q channels. Dataset I was the collected frequency-hopping dataset, and dataset II was the collected fixed-frequency dataset. Datasets I and II used different types of radiation source radio stations. However, the source radio stations in the same dataset were of the same type. The receiver model was RSA6120A. In the sample dataset, the signals transmitted by all radio stations were random. Therefore, the baseband signals transmitted by different radiation source stations of the same model differed. The baseband signals include in-phase signals and quadrature signals.

Dataset I: Signals were collected from eight emitters that transmit signals with quadrature phase shift keying modulation. The hopping frequency range was 450–460 MHz, and data were acquired every 1 MHz. The specific parameters are listed in Table 3.

Table 3
Dataset I signal parameters

Signal parameter	Parameter value
Signal carrier frequency	450–460 MHz
Modulation	QPSK
Operating mode	Voice
Code rate	256 Kbps
Sampling rate	50 MHz
Radio power	0.125 W

Dataset II: Signals were collected from nine emitters with carrier frequencies of 450 MHz and 512 MHz, respectively. A signal and spectrum analyzer connected to an antenna received the signals, converting the RF signals to the baseband. The specific parameters are presented in Table 4.

Table 4
Dataset II signal parameters

Signal parameter	Parameter value
Signal fixed frequency	450/512 MHz
Modulation	8 PSK
Code rate	512 Kbps
Sampling rate	3.84 MHz
Signal-to-noise ratio	>15 dB
Sampling time	≈ 2 s

Data preprocessing consists of three parts: data segmentation, signal filtering, and standardization.

- Because the original signal has transmission silence time and the sample data of the silence time cannot reflect the personal characteristics of the radiation source, a reasonable threshold was set. When the variance of the sample signal value over a period of time was less than the specified threshold value, the signal sample was considered to be silent during this period and was discarded.
- The processed dataset was sliced according to a fixed length, and datasets I and II were divided into several samples with a length of 8192 sampling points.
- To avoid the impact of signal power difference on the identification effect, it is necessary to standardize the sample data because there is a certain difference in the transmitting signal power of different stations collected by the receiving equipment. In addition, the data of each sample in the sequence were subtracted from the mean value and divided by the standard deviation so that the mean value of all sample data was zero and the variance was one.

4.2. Network parameters and comparative experimental settings

We set the main parameters of the network model as presented in Table 5.

Table 5
Model main parameter setting

Signal parameter	Parameter value
epoch	200
Batch size	64
Optimizer	Adam
Loss function	Cross Entropy

The learning rate was initially 10^{-3}, and it was reduced to one-tenth for every 100 epochs. We used the ResNet18 and ResNet34 algorithms as comparison algorithms; they were both converted from a 2D form, and the main parameter settings of the network parameters were the same. In addition, to study the influence of the AM, this study also used the CVResNet-1D model (with the attention unit removed) for comparison purposes (Table 6).

Table 6
Number of parameters and training time per epoch

Model	ResNet18	ResNet34	CVResNet -1D	CVResNet -1D-AM
Number of parameters	3848456	7222792	3619912	3628118
Time per epoch	37 s	58 s	55 s	56 s

4.3. Frequency-hopping dataset identification results

Dataset I: We randomly selected 2000 samples as the training sample set and 200 samples as the test sample set from the

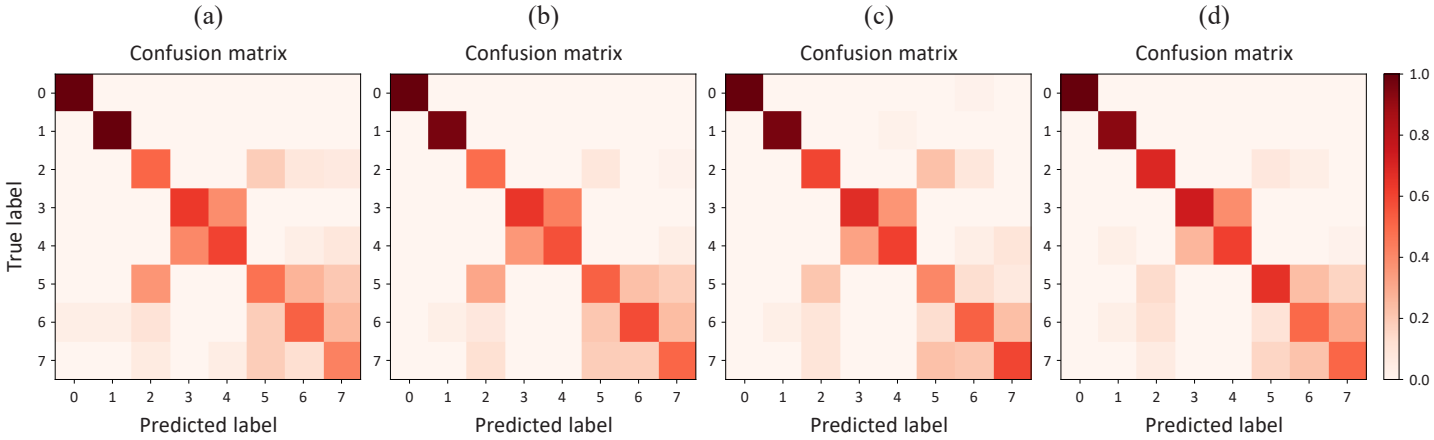

Fig. 8. Confusion matrix results. a) ResNet18 obfuscation matrix, b) ResNet34 obfuscation matrix, c) complex-valued residual networks one-dimensional (CVResNet-1D) obfuscation matrix, and d) CVResNet-1D-attention mechanism (AM) obfuscation matrix

preprocessed segmented frequency-hopping data sample set of each radio station; we independently conducted five experiments, in which a new set of random data was selected in each experiment, and the random data used in each experiment were different. Through the five independent experiments, the contingency and specificity of the experimental results were avoided. The identification effect was compared as shown in Table 7.

Table 7
Identification accuracy on Dataset I

Identification algorithm	Identification accuracy
ResNet18	87.56%
ResNet34	89.18%
CVResNet-1D	89.52%
CVResNet-1D- AM	92.12%

The results of the confusion matrix for the four algorithms are shown in Fig. 8. From the confusion matrix, it can be observed that stations 1 and 2 yielded the best identification effects for the eight stations in dataset I, and the error probabilities of stations 5 and 8 were higher. Subject to the condition of the same number of network parameters, the identification accuracy of the CVResNet-1D identification algorithm was higher than that of the ResNet18 algorithm, and the identification effect of the eight stations was better. For the same number of network layers, the identification accuracies of the ResNet34 and CVResNet-1D algorithms were similar, but the network parameters of the ResNet34 algorithm were much larger than those of the CVResNet-1D algorithm. In addition, from the experimental results, we found that the CVResNet-1D-AM algorithm, which combined the CVResNet-1D algorithm and the AM, can significantly improve the identification accuracy of the algorithm with the use of a small number of network parameters.

To further compare the effects of several identification algorithms, we added Gaussian white noise to dataset II and changed the signal-to-noise ratio condition of the sample set to obtain fixed-frequency datasets with different signal-to-noise ratio conditions.

4.4. Influence of different signal-to-noise ratios on identification accuracy

Dataset II: We randomly selected 500 samples from the preprocessed segmented data sample set of each station as the training sample set, and 100 samples as the test sample set to change the signal-to-noise ratio condition by adding Gaussian white noise (–10 dB, –9 dB, ..., –1 dB), and we independently conducted five experiments, in which a new set of random data was selected in each experiment, and the random data used in each experiment were different. Finally, the identification results' average accuracy was compared, as shown in Table 8 and Table 9.

We found that adding Gaussian white noise to simulate different communication channel environments increased

Table 8
Identification accuracy on Dataset II at 450 MHz

Algorithm	–10	–9	–8	–7	–6	–5	–4	–3	–2	–1
ResNet18	54.04	57.65	68.61	75.18	80.42	84.57	89.68	92.34	95.10	96.06
ResNet34	50.54	58.93	65.53	71.06	78.61	84.32	88.19	93.40	94.14	97.44
CVResNet-1D	57.23	62.76	68.82	74.57	80.21	85.53	89.78	94.46	96.48	97.65
CVResNet-1D-AM	**57.65**	**64.57**	**69.36**	**77.44**	**84.46**	**87.76**	**92.76**	**95.64**	**97.44**	**98.82**

Table 9
Identification accuracy on Dataset II at 512 MHz

Algorithm	–10	–9	–8	–7	–6	–5	–4	–3	–2	–1
ResNet18	41.32	47.06	53.83	65.82	67.92	73.18	80.54	86.54	92.63	97.27
ResNet34	41.14	47.42	51.31	63.30	71.82	75.28	86.43	88.64	94.74	96.95
CVResNet-1D	**47.10**	49.00	57.30	69.40	72.87	79.28	86.96	86.43	95.37	97.05
CVResNet-1D-AM	46.80	**50.26**	**58.16**	**70.56**	**74.97**	**81.80**	**89.06**	**90.22**	**96.21**	**97.68**

the probability of misclassification of several identification algorithms and the identification accuracy decreased in a low signal-to-noise ratio environment. The experimental results showed that compared with the real residual network, we found that the complex residual network is more robust because it can extract the relevant information between the in-phase and quadrature components of the radio frequency baseband signal. If the AM is added between the complex residual stack and the fully connected layer, it can suppress the invalid features caused by noise; thus, the weight of the network parameters can focus on the part that reflects the fingerprint characteristics of the radio station to improve the effect of classification and identification.

5. CONCLUSIONS

In this paper, we proposed a new CVResNet-1D-AM algorithm for the signal identification of communication radiation sources. In particular, the designed 1D, complex-valued residual convolutional layer can directly extract features from the time-domain sequence of the communication radiation source signal. The AM unit was integrated into the CVResNet-1D model to improve the identification accuracy of the neural network. The experimental results show that, compared with the real-numbered domain deep learning method, the CVResNet-1D-AM algorithm was associated with a smaller number of classification errors and was able to perform and yield better identification outcomes for the same network parameter conditions. In future work, we will optimize the CVResNet-1D-AM model for the communication radiation source signal to further improve identification accuracy.

ACKNOWLEDGEMENTS

The authors would like to acknowledge the support of Anhui Provincial Natural Science Foundation (No. 1908085MF202) and Independent Scientific Research Program of National University of Defense Science and Technology (No.ZK18-03-14).

REFERENCES

[1] K. Talbot, P. Duley, and M. Hyatt, "Specific emitter identification and verification," *Technol. Rev. J.*, vol. Spring/Summer, pp. 113–133, 2003.

[2] G. Baldini, G. Steri, and R. Giuliani, "Identification of wireless devices from their physical layer radio-frequency fingerprints," in *Encyclopedia of Information Science and Technology*, 4th Ed., 2018, ch. 533, pp. 6136–6146.

[3] G. Huang, Y. Yuan, X. Wang, and Z. Huang, "Specific emitter identification based on nonlinear dynamical characteristics," *Can. J. Electr. Comput. Eng.*, vol. 39, no. 1, pp. 34–41, 2016, doi: 10.1109/cjece.2015.2496143.

[4] Y. Pan, H. Peng, T. Li, and W. Wang, "High-fidelity symbol synchronization for specific emitter identification," in *2019 IEEE 3rd Information Technology, Networking, Electronic and Automation Control Conference (ITNEC)*, 15–17 March 2019, pp. 393–398, doi: 10.1109/ITNEC.2019.8729181.

[5] S. Ching-Sung and L. Chin-Teng, "A vector neural network for emitter identification," *IEEE Trans. Antennas Propag.*, vol. 50, no. 8, pp. 1120–1127, 2002, doi: 10.1109/TAP.2002.801387.

[6] R. Klein, M.A. Temple, M.J. Mendenhall, and D.R. Reising, "Sensitivity Analysis of Burst Detection and RF Fingerprinting Classification Performance," in *2009 IEEE International Conference on Communications*, 14–18 June 2009, pp. 1–5, doi: 10.1109/ICC.2009.5199451.

[7] O. Ureten and N. Serinken, "Bayesian detection of Wi-Fi transmitter RF fingerprints," *Electron. Lett.*, vol. 41, no. 6, pp. 373–374, 2005, doi: 10.1049/el:20057769.

[8] J. Hall, M. Barbeau, and E. Kranakis, "Radio frequency fingerprinting for intrusion detection in wireless networks," *IEEE Trans. Dependable Secure Comput.*, vol. 12, pp. 1–35, 2005.

[9] S. Guo, S. Akhtar, and A. Mella, "A Method for Radar Model Identification using Time-domain Transient Signals," *IEEE Transactions on Aerospace and Electronic Systems*, pp. 1–1, 2021, doi: 10.1109/TAES.2021.3074129.

[10] Y. Yuan, Z. Huang, H. Wu, and X. Wang, "Specific emitter identification based on Hilbert–Huang transform-based time–frequency–energy distribution features," *IET Commun.*, vol. 8, no. 13, 2404–2412, 2014.

[11] U. Satija, N. Trivedi, G. Biswal, and B. Ramkumar, "Specific emitter identification based on variational mode decomposition and spectral features in single hop and relaying scenarios," *IEEE Trans. Inf. Forensics Secur.*, vol. 14, no. 3, pp. 581–591, 2019, doi: 10.1109/tifs.2018.2855665.

[12] L. Li, H. B. Ji, and L. Jiang, "Quadratic time-frequency analysis and sequential recognition for specific emitter identification," *IET Signal Proc.*, vol. 5, pp. 568–574, 2011, doi: 10.1049/iet-spr.2010.0070.

[13] J. Zhang, F. Wang, Z. Zhong, and O. Dobre, "Novel Hilbert Spectrum-Based Specific Emitter Identification for Single-Hop and Relaying Scenarios," in *2015 IEEE Global Communications Conference (GLOBECOM)*, 6–10 Dec. 2015 2015, pp. 1–6, doi: 10.1109/GLOCOM.2015.7417299.

[14] Z. Tang and S. Li, "Steady Signal-Based Fractal Method of Specific Communications Emitter Sources Identification," in *Wireless Communications, Networking and Applications*, Q.-A. Zeng, Ed., Springer India, New Delhi, 2016, pp. 809–819, doi: 10.1007/978-81-322-2580-5_73.

[15] F. Zhuo, Y. Huang, and J. Chen, "Radio frequency fingerprint extraction of radio emitter based on I/Q imbalance," *Procedia Comput. Sci.*, vol. 107, pp. 472–477, 2017, doi: 10.1016/j.procs.2017.03.092.

[16] G. Huang, Y. Yuan, X. Wang, and Z. Huang, "Specific emitter identification based on nonlinear dynamical characteristics," *Can. J. Electr. Comput. Eng.*, vol. 39, pp. 34–41, 2016, doi: 10.1109/CJECE.2015.2496143.

[17] M. Liu and J.F. Doherty, "Specific emitter identification using nonlinear device estimation," in *2008 IEEE Sarnoff Symposium*, 28–30 April 2008, pp. 1–5, doi: 10.1109/SARNOF.2008.4520119.

[18] M. Liu and J.F. Doherty, "Nonlinearity estimation for specific emitter identification in multipath channels," *IEEE Trans. Inf. Forensics Secur.*, vol. 6, no. 3, pp. 1076–1085, 2011, doi: 10.1109/TIFS.2011.2134848.

[19] J. Dudczyk and A. Kawalec, "Specific emitter identification based on graphical representation of the distribution of radar signal parameters," *Bull. Pol. Acad. Sci. Tech. Sci.*, vol. 63, no. 2, pp. 391–396, 2015, doi: 10.1515/bpasts-2015-0044.

[20] Y. Zhao, L. Wu, J. Zhang, and Y. Li, "Specific emitter identification using geometric features of frequency drift curve," *Bull. Pol. Acad. Sci. Tech. Sci.*, vol. 66, pp. 99–108, 2018, doi: 10.24425/119063.

[21] Ł. Rybak and J. Dudczyk, "A geometrical divide of data particle in gravitational classification of moons and circles data sets," *Entropy*, vol. 22, p. 16, 2020, doi: 10.3390/e22101088.

[22] J. Han, T. Zhang, D. Ren, and X. Zheng, "Mechanism analysis and feature extraction algorithm of communication emitter fingerprint," *AEU Int. J. Electron. Commun.*, vol. 106, 2019, doi: 10.1016/j.aeue.2019.04.020.

[23] M.K.M. Fadul, D.R. Reising, and M. Sartipi, "Identification of OFDM-based radios under rayleigh fading using RF-DNA and deep learning," *IEEE Access*, vol. 9, pp. 17100–17113, 2021, doi: 10.1109/ACCESS.2021.3053491.

[24] J. Dudczyk, "A method of feature selection in the aspect of specific identification of radar signals," *Bull. Pol. Acad. Sci. Tech. Sci.*, vol. 65, pp. 113–119, 2017, doi: 10.1515/bpasts-2017-0014.

[25] K. Sa, D. Lang, C. Wang, and Y. Bai, "Specific emitter identification techniques for the internet of things," *IEEE Access*, vol. 8, pp. 1644–1652, 2020, doi: 10.1109/ACCESS.2019.2962626.

[26] Y. Pan, S. Yang, H. Peng, T. Li, and W. Wang, "Specific emitter identification based on deep residual networks," *IEEE Access*, vol. 7, pp. 54425–54434, 2019, doi: 10.1109/ACCESS.2019.2913759.

[27] L.J. Wong, W.C. Headley, S. Andrews, R.M. Gerdes, and A.J. Michaels, "Clustering learned CNN features from raw I/Q data for emitter identification," in *MILCOM 2018 – 2018 IEEE Military Communications Conference (MILCOM)*, 29–31 Oct. 2018, pp. 26–33, doi: 10.1109/MILCOM.2018.8599847.

[28] M. Zhang, M. Diao, and L. Guo, "Convolutional neural networks for automatic cognitive radio waveform recognition," *IEEE Access*, vol. 5, pp. 11074–11082, 2017, doi: 10.1109/ACCESS.2017.2716191.

[29] N.E. West and T.O. Shea, "Deep architectures for modulation recognition," in *2017 IEEE International Symposium on Dynamic Spectrum Access Networks (DySPAN)*, 6–9 March 2017, pp. 1–6, doi: 10.1109/DySPAN.2017.7920754.

[30] Q. Wu *et al.*, "Deep learning based RF fingerprinting for device identification and wireless security," *Electron. Lett.*, vol. 54, pp. 1405–1407, 2018, doi: 10.1049/el.2018.6404.

[31] L. Ding, W. Shilian, F. Wang, and W. Zhang, "Specific emitter identification via convolutional neural networks," *IEEE Commun. Lett.*, vol. 22, no. 12, pp. 2591–2594, 2018, doi: 10.1109/LCOMM.2018.2871465.

[32] G. Baldini, C. Gentile, R. Giuliani, and G. Steri, "A comparison of techniques for radiometric identification based on deep convolutional neural networks," *Electron. Lett.*, vol. 55, pp. 90–92, 2018, doi: 10.1049/el.2018.6229.

[33] K. Huang, J. Yang, H. Liu, and P. Hu, "Deep adversarial neural network for specific emitter identification under varying frequency," *Bull. Pol. Acad. Sci. Tech. Sci.*, vol. 69, no. 2, p. e136716, 2021, doi: 10.24425/bpasts.2021.136737.

[34] B. Wu, S. Yuan, P. Li, Z. Jing, S. Huang, and Y. Zhao, "Radar emitter signal recognition based on one-dimensional convolutional neural network with attention mechanism," *Sensors*, vol. 20, p. 6350, 2020, doi: 10.3390/s20216350.

[35] T.J. Shea and N. West, "Radio Machine Learning Dataset Generation with GNU Radio," *Proceedings of the GNU Radio Conference*, vol 1, no.1, 2016. [Online]. Available: https://pubs.gnuradio.org/index.php/grcon/article/view/11.

[36] T.J. O'Shea, T. Roy, and T.C. Clancy, "Over-the-Air deep learning based radio signal classification," *IEEE J. Sel. Top. Signal Process.*, vol. 12, no. 1, pp. 168–179, 2018, doi: 10.1109/JSTSP.2018.2797022.

[37] A. Hirose and S. Yoshida, "Generalization characteristics of complex-valued feedforward neural networks in relation to signal coherence," *IEEE Trans. Neural Networks*, vol. 23, pp. 541–551, 2012, doi: 10.1109/TNNLS.2012.2183613.

[38] C. Trabelsi *et al.*, "Deep complex networks," presented at *the ICLR 2018*, 2018.

[39] Y. Ying and J. Li, "Radio frequency fingerprint identification based on deep complex residual network," *IEEE Access*, vol. 8, pp. 204417–204424, 2020, doi: 10.1109/ACCESS.2020.3037206.

[40] S. Woo, J. Park, J.-Y. Lee, and I.S. Kweon, "CBAM: Convolutional Block Attention Module," in *Computer Vision – ECCV 2018*, Cham, V. Ferrari, M. Hebert, C. Sminchisescu, and Y. Weiss, Eds., Springer International Publishing, 2018, pp. 3–19.